First-principles study of carbon capture and storage properties of porous MnO_2 octahedral molecular sieve OMS-5

Matthew Lawson,[1] Jarod Horn,[2] Winnie Wong-Ng,[2] Laura Espinal,[2] Saul H. Lapidus,[3] Huong Giang Nguyen,[2] Yongtao Meng,[4] Steven L. Suib,[4,5] James A. Kaduk,[6] and Lan Li[1,7,a)]

[1]*Micron School of Materials Science and Engineering, Boise State University, Boise, Idaho 83706*
[2]*Materials Measurement Science Division, National Institute of Standards and Technology, Gaithersburg, Maryland 20899*
[3]*Department of Chemistry, Illinois Institute of Technology, Chicago, Illinois 60616*
[4]*Department of Physics, North Central College, Naperville, Illinois 60540*
[5]*Institute of Materials Science, University of Connecticut, Storrs, Connecticut 06269*
[6]*Advanced Photon Source, Argonne National Laboratory, Argonne, Illinois 60439*
[7]*Center for Advanced Energy Studies, Idaho Falls, Idaho 83401*

(Received 25 October 2018; accepted 3 January 2019)

Based on the experimentally determined framework structure of porous MnO_2 octahedral molecular sieve (OMS)-5, we used density functional theory-based calculations to evaluate the effect of Na^+ cation on pore dimensionality and structural stability, and the interaction between CO_2 and OMS-5. We quantified the formation energy of one CO_2/unit tunnel and two CO_2/unit tunnel, and projected the electronic density of states on the OMS-5 framework, CO_2 molecules, and Na^+ cations to reveal their individual contributions and bonding nature. Partial charge densities were also calculated to investigate CO_2 adsorption behavior in the OMS-5. Our studies predict the initial stage and driving force for the adsorption of CO_2 in the OMS-5, guiding the OMS material design for carbon capture and storage applications. © *2019 International Centre for Diffraction Data.*
[doi:10.1017/S0885715619000010]

Key words: carbon capture and storage, porous solid, octahedral molecular sieve, first-principles studies, density functional theory

I. INTRODUCTION

Because of rising energy demands, the production of CO_2 emissions is increasing at alarming rates (Jenkinson *et al.*, 1991; Holtz-Eakin and Selden, 1995; MacKellar *et al.*, 1995; Lakshmanan and Han, 1997; Raupach *et al.*, 2007; Botzen *et al.*, 2008). To counteract the exponential increase of flue gas (combustion exhaust containing nitrogen and CO_2), current methods employ aqueous solutions of alkanolamine-based solvents (Rochelle, 2009). The amine scrubbers absorb CO_2, and then water vapor is boiled off, leaving the captured CO_2. This method is effective but expensive (Rao and Rubin, 2002; D'Alessandro *et al.*, 2010). Hence adsorbent materials, such as metal-organic frameworks (MOFs) (Caskey *et al.*, 2008) and octahedral molecular sieves (OMS) (Espinal *et al.*, 2012), are also being explored. MOFs are a more recent discovery with high CO_2 selectivity, but the diffusion mechanism of gases in the MOFs is still not well studied (D'Alessandro *et al.*, 2010). Therefore, the OMS series poses as another potential solution to efficiently capture CO_2.

OMS is comprised of the columns of edge-sharing of MnO_6 octahedra. MnO_2 can form an infinite number of OMS structures with alternating 1×1 tunnels and $m \times n$ tunnels. Suib and co-workers first synthesized thermally stable OMS-1, comprised of a 3×3 (i.e. $m = 3$, $n = 3$) manganese oxide structure with a pore size of 6.9 Å (Shen *et al.*, 1993). Their work then focused on determining how the morphology of OMS-1 could be controlled. Shortly after, new morphology OMS-2 was synthesized. OMS-2 is known as α-MnO_2 and is comprised of edge-sharing MnO_6 octahedra forming a 2×2 tunnel structure (i.e. $m = 2$, $n = 2$) and reducing the pore size to 4.6 Å (DeGuzman *et al.*, 1994). As synthesis techniques improved, the tunnel arrangements began to vary. A 2×4 tunnel structure (i.e. $m = 2$, $n = 4$) with pore sizes of 4.6 Å × 9.2 Å, i.e. OMS-5, was discovered (Shen *et al.*, 2005; Zhang *et al.*, 2014). In addition, doping MnO_x with metal cations has been shown to improve electronic and catalytic performance (Suib and Iton, 1994; Suib, 1998; Hou *et al.*, 2013), and can also serve as templates for OMS synthesis (Liu *et al.*, 2003; Shen *et al.*, 2005).

Accomodating cations, such as Na^+, K^+, Ba^{2+}, Ca^{2+}, facilitates the stability of the equilibrium of the porous OMS materials. The tunnel structures of the OMS materials are potentially used as adsorbents for gas separation and storage. The guest/host separation efficiency depends on pore features, such as pore shape and size, and interaction between gas molecules and pore surface. For carbon capture and storage aplications, the selectivity of CO_2 from a mixture of gases can be tuned by controlling the pore features of the OMS materials. The type and charge of cations doped in the OMS materials are found to affect both pore features and CO_2 selectivity.

Because of its pore size of 4.6 Å being comparable to the kinetic diameter of 3.3 Å for CO_2, OMS-2 has been considered for use in carbon capture and storage. Our previous

a)Author to whom correspondence should be addressed. Electronic mail: lanli@boisestate.edu

studies applied first-principles density functional theory (DFT)-based calculations to comprehensively explore its atomic, electronic, and magnetic properties; cation, water, and other hydrate effects; CO_2 adsorption; and diffusion mechanisms. As seen in Figure 1, the lowest-energy structure of cation-doped $Mn_{24}O_{48}$ consisted of alternating 1×1 and 2×2 tunnels, where the cation was energetically positioned in the 2×2 tunnel because of the larger space (Cockayne and Li, 2012). Because of Mn^{4+} ions, the Mn–Mn coupling between corner-sharing MnO_6 was antiferromagnetic while the interactions between edge-sharing octahedra in neighboring columns were weakly ferromagnetic. The antiferromagnetic interactions were stronger, so the quasi-one-dimensional units were formed by the four columns of MnO_6 octahedra that surrounded a 1×1 tunnel. The presence of cations could affect the charge of Mn. Local density of state (LDoS) calculations exhibited the electron donation from cations to MnO_2. The donated electrons were shared by neighboring Mn atoms, resulting in the reduction of an appropriate amount of Mn^{4+} to Mn^{3+} in order to maintain charge balance. According to experimental observations, the synthesis of OMS-2 incorporated water or other hydrates in the sample. DFT calculations clarified that those species formed a weak bond to a cation because of dipole–ion interactions. It should be easy to completely dehydrate the sample without impacting the cation in order to increase the adsorption uptake of CO_2 in the OMS-2.

Through DFT-based energetic calculations, we further predicted CO_2 adsorption and diffusion mechanisms in the OMS-2 and compared the effects of different cations, such as K^+, Na^+, and Ba^{2+}. The doped cations present in OMS-2 not only stabilized its porous structure but also tailored CO_2–pore interaction. We firstly focused on the K^+ cation. Our previous experiments exhibited CO_2 sorption hysteresis, where the adsorption isotherm curve of CO_2 uptake differed from that of the desorption curve (Espinal *et al.*, 2012). At a temperature of 303 K, a significant hysteresis existed between the adsorption and desorption isotherm paths. The width of the hysteresis loop also increased with equilibrium time. However, the hysteresis only occurred when the pressure exceeded 7 bar. Experiments suggested that the OMS-2 material was able to capture CO_2, but had a difficulty releasing CO_2 above 7 bars. These results raised crucial questions related to CO_2 adsorption and diffusion mechanisms and the driving force for the hysteresis. DFT-based energetic calculations indicated that the hysteresis could be explained by the presence of K^+ cations acting as "gate keepers" hindering the diffusion of CO_2 in the 2×2 tunnels of OMS-2. A large activation energy was required for CO_2 in a low concentration to bypass K^+, so CO_2 would diffuse until it encountered K^+ and then remained at an optimum distance from K^+. Upon desorption, CO_2 could easily exit the tunnel with no hysteresis, in agreement with experimental observations below 7 bar. Increasing CO_2 concentration with pressure could dramatically decrease the activation energy required for CO_2 diffusion deep in the OMS-2 tunnel, in agreement with experimental observations above 7 bar. However, upon desorption CO_2 had to overcome the high-energy barrier to pass through K^+ in reverse, resulting in hysteretic behavior. In addition, the high concentration of CO_2 possibly caused the formation of stable carbonate-like complexes because of the limited space of the OMS-2 tunnel and dipole interactions between CO_2 molecules (Li *et al.*, 2013).

In comparison between K^+ and other types of cations, we found the charge, type, and mobility of the cation could affect not only the OMS-2 structural features but also CO_2 sorption performance, implying that modifying these features could optimize the carbon capture properties of OMS-2. We extended our DFT-based energetic and electronic structure calculations to Na^+ and Ba^{2+} cations for comparison with K^+ (Williamson *et al.*, 2015). Because of the higher charge and more electrons donated to the MnO_2, Ba^{2+} had a more than twice stronger interaction with the OMS-2 porous surface than both K^+ and Na^+ did. However, the Ba-doped OMS-2 would have the lower CO_2 uptake because of the stronger Ba–MnO_2 interaction and the higher activation energy for CO_2 to bypass Ba^{2+} for further diffusion. We then predicted that Na^+ would have the best CO_2 uptake performance for two key reasons. One was the relatively weaker Na–MnO_2 interaction, while the second was a high mobility of Na^+ in the OMS-2 tunnel. When CO_2 encountered Na^+, it would continue diffusing by pushing Na^+ aside. This scenario could not only enhance the CO_2 uptake amount but also improve its adsorption–desorption hysteresis. Finally, we summarized three possible diffusion mechanisms for CO_2 in the OMS-2 tunnel, depending on the activation energy barrier for further CO_2 diffusion and cation mobility. Scenario I involved CO_2 kinetically trapped in an equilibrium position with no further diffusion. Scenario II was to bypass the cation to further diffuse along the OMS-2 tunnel. Scenario III was to continue diffusing by pushing the cation aside. We suggested that Scenarios I and II would occur in the K-doped OMS-2 sample because of the relatively low activation energy barrier for CO_2 at high concentration to bypass K^+. With the high mobility of Na^+, Scenarios I and III would be

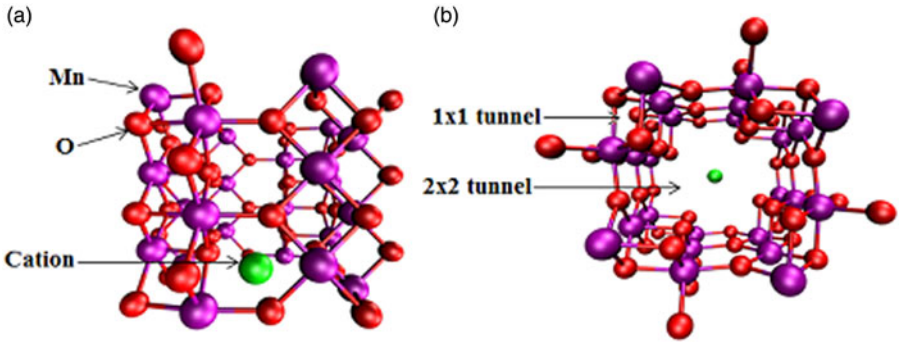

Figure 1. (Color online) OMS-2 with alternating 1×1 and 2×2 tunnels, accommodating with a cation in the 2×2 tunnel, with Mn in purple, O in red, and cation in green. (a) Side view of a single cell, and (b) a single cell down tunnel axes.

favorable in the Na-doped OMS-2 sample. The strong Ba–MnO_2 interaction suggested that only Scenario I occurs in the Ba-doped OMS-2. We also predicted that Na-doped OMS-2 should have the highest CO_2 uptake, followed by the K-doped OMS-2, and finally Ba-doped OMS-2.

Our previous studies suggested that we could control CO_2 sorption hysteresis and uptake by optimizing the chemistry, size, and concentration of cations accommodated in the OMS-2 tunnel, and Na^+ had the best CO_2 sorption performance. As a follow-up, this paper emphasizes our computational efforts to study OMS-5 with the larger size of tunnels (i.e. $m = 2$ and $n = 4$) and determine how cations affect CO_2 sorption in the tunnels. OMS-5 is expected to intake a larger amount of CO_2 because of its larger pore size, but it could lead to different CO_2 sorption mechanisms. Besides DFT-based energetic and electronic structural calculations, we further performed partial charge density analyses to advance our understanding on the nature of bonding among OMS-5, Na^+ cations, and CO_2 molecules.

II. METHODS

We continued conducting DFT-based studies of OMS-5 with the bigger pore size, Na^+ cation dopants, and CO_2 adsorption. Because of Mn^{4+}, we first found the lowest-energy magnetic state of OMS-5, as shown in Figure 2. Mn atoms have an antiferromagnetic interaction with the magnetic moments of ±4 μB. To account for the dipole–dipole interactions, van der Waals forces were also considered by applying the D2 method of Grimme (Grimme, 2006). A plane-wave cutoff energy of 300 eV was implemented with the spin-polarized generalized gradient approximation (GGA) and Perdew–Burke Ernzerhof (Perdew *et al.* 1996) exchange-correlation functional. For strongly correlated element Mn, we used the GGA + U approach by Liechtenstein *et al.* (1995), with the effective on-site Coulomb value (U) of 2.8 eV and the effective on-site exchange (J) value of 1.2 eV for Mn (Li *et al.*, 2013). Cell and atomic positions were fully relaxed until the residual forces reached 0.01 eV $Å^{-1}$. The ground-state unit cell consists of lattice parameters $a = 12.353$ Å, $b = 2.708$ Å, and $c = 23.050$ Å. We then extended the unit cell along the b axis (i.e. the tunnel axis) by four times to form a $Mn_{96}O_{192}$ compound in order to accommodate CO_2 molecules in the 2 × 4 tunnels.

Our previous work with OMS-2 showed that cations could stabilize not only the tunnel size and shape of the porous structure, but also play a role as a "gate keeper" to induce an energy barrier for CO_2 to diffuse along the tunnel (Williamson *et al.*, 2015). The larger tunnel size of the OMS-5 structure would undoubtedly affect its adsorption mechanism of CO_2, so we focus on three following scenarios:

- **Scenario I:** OMS-5 without cations
- **Scenario II:** OMS-5 with a low concentration of Na^+ cations
- **Scenario III:** OMS-5 with a high concentration of Na^+ cations

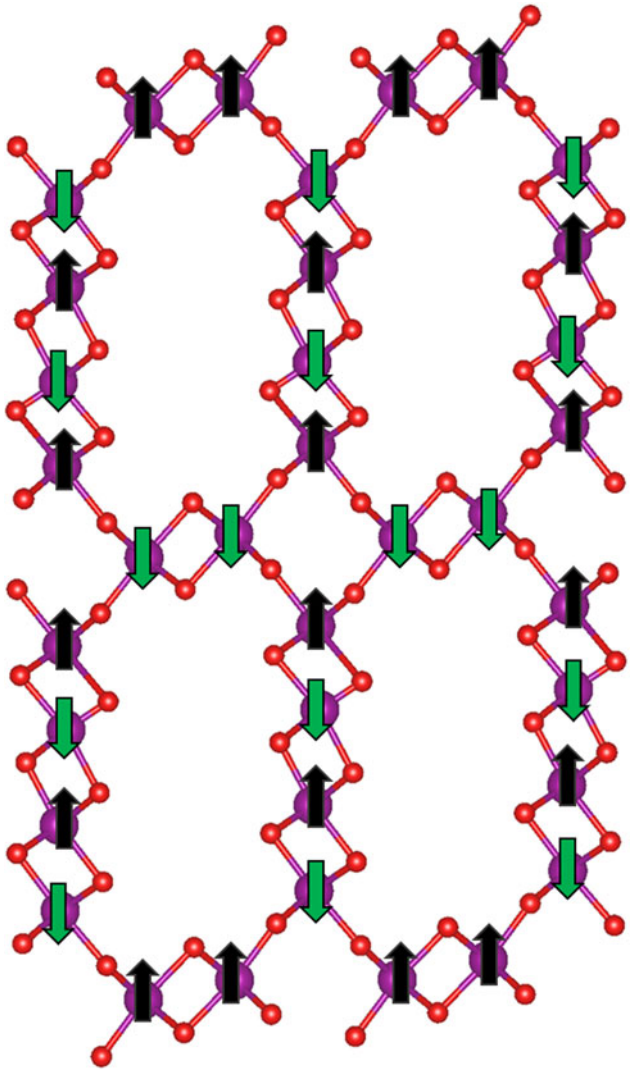

Figure 2. (Color online) Unit cell of OMS-5 with alternating 1 × 1 and 2 × 4 tunnels. Spin states "up" in black and "down" in dark green are applied to Mn atoms in purple. O atoms are represented in red.

For comparison, a low concentration refers to one Na^+ cation for each 2 × 4 tunnel, i.e. $Mn_{96}O_{192}Na_4$ while a high concentration is two Na^+ cations per 2 × 4 tunnel, i.e. $Mn_{96}O_{192}Na_8$. In this study, we are primarily interested in how stability of the OMS-5 structure changes as the concentration of Na^+ changes in each pore. There are two possible orientations of CO_2 molecules in the tunnels, including the "head-to-head" orientation, where the CO_2 molecules align linearly along the tunnel, and the "stacked" orientation, where the CO_2 molecules stack on top of each other in the tunnel. We evaluated the stability of Na^+ or CO_2 in the OMS-5 tunnel by calculating its formation energy E_f, as follows:

$$E_f = \frac{E_{\text{OMS-5 with Na or CO}_2} - E_{\text{OMS-5 without Na or CO}_2} - N_{\text{Na or CO}_2} * E_{\text{Na or CO}_2}}{N_{\text{Na or CO}_2}} \quad (1)$$

$E_{\text{OMS-5 with Na or CO}_2}$ and $E_{\text{OMS-5 without Na or CO}_2}$ represent the total energies for OMS-5 with and without Na^+ or CO_2

added, respectively. $N_{Na\ or\ CO_2}$ is the total number of Na^+ or CO_2 added. $E_{Na\ or\ CO_2}$ is an energy of individual Na^+ or CO_2. If E_f is a negative value, it refers to a binding energy, indicating that the configuration is energetically stable. If E_f is a positive value, it refers to an energy penalty to form the configuration, which is relatively unstable.

Density of states (DoS) was also calculated to provide insight into electronic interactions and Na^+ cation effects. The electronic contributions of the OMS-5 framework, CO_2 molecules, and Na^+ cations were then projected on the LDoS. Finally, the partial charge densities were calculated for the electronic energy range between −5 eV and the Fermi energy to study the bonding characteristics of the CO_2 molecules and OMS-5 framework on the electronic scale. This energy range was chosen to analyze the distribution of valence electrons on the atomic sites.

III. RESULTS AND DISCUSSION

A. OMS-5 structure

Figure 3 shows three scenarios for studying the CO_2 adsorption/desorption mechanism, including OMS-5 without cations (i.e. Scenario I $Mn_{96}O_{192}$), with a low concentration of Na^+ cations (i.e. Scenario II $Mn_{96}O_{192}Na_4$), and with a high concentration of Na^+ cations (i.e. Scenario III $Mn_{96}O_{192}Na_8$) to determine cation effects on the structural stability of OMS-5. In Scenario I, Mn–O bond lengths are approximately 1.9 Å. In Scenario II, adding four Na^+ cations would allow for a single cation in each 2 × 4 tunnel. Na^+ does not always stay in the middle of the tunnel. Its position depends on the size and shape of the pore. Interestingly, the Mn–O bonds close to Na^+ can retain bond lengths of 1.9 Å, while the Mn–O bonds far from Na^+ have a significant change in their bond lengths, ranging from 1.82 to 1.92 Å. In Scenario III, the large pore size of OMS-5 could accommodate two Na^+ cations in each 2 × 4 tunnel. Na–Na distances are approximately 4.8 Å. Similar to Scenario II, the change of the Mn–O bond lengths depends on the position of Na^+. Table I shows that the lattice parameters of OMS-5 for all three scenarios do not change significantly. In comparison between Scenarios I and II, adding Na^+ slightly increases the *a* and *c* lattice parameters by 0.1 and 0.5%, respectively, while the *b* lattice parameter decreases 0.7%. Similarly, in comparison between Scenarios I and III, adding more Na^+ increases the *a* and *c* lattice parameters by 0.07 and 0.5%, respectively, and decreases the *b* lattice parameter by 0.8%. Obviously, the change of <1% in each lattice parameter could be negligible. With $\beta = \sim 97^0$ and $\alpha = \gamma = \sim 90°$, the OMS-5 cell remains monoclinic in the presence of Na^+ cations. However, the cell volume shrinks by 0.3% with a low concentration of Na^+ cations and 0.8% with a high concentration of Na^+ cations, which also happens in the OMS-2 materials (Williamson *et al.*, 2015). The volume decrease is the concequence of the shorter tunnel length along the *b* axis. The tunnel size, i.e. $a \times c$ or pore size, remains the same. Our computational results suggest that the presence of Na^+ slightly shrinks the cell volume, but it maintains the pore size and shape.

Using Eq. (1), we could determine the stability of Na^+ cations accommodated in the OMS-5 tunnels. The corresponding formation energy per Na^+ cation is listed in Table II. In the low concentration $Mn_{96}O_{192}Na_4$, the formation energy of a Na^+ cation is −2.10 eV/Na^+. This negative value indicates that the presence of Na^+ is stable, and Na^+ forms a strong bond with the OMS-5 framework. As its concentration increases, the formation energy of a Na^+ cation gradually increases and becomes less negative. For $Mn_{96}O_{192}Na_8$, its formation energy is 0.44 eV/Na^+. The positive value represents an energy penalty for incorporating an additional Na^+ cation in each 2 × 4 tunnel. As a result, the presence of a single Na^+ in each pore stabilizes the porous structure of OMS-5, but it costs energy to incorporate an additional Na^+ in each pore. Thus, a low concentration of Na^+ is more energetically favorable. To further study the interaction between Na^+ and OMS-5, we projected electronic DoS on the OMS-5 before and after adding Na^+ cations. Figure 4 shows that the DoS of OMS-5 before adding Na^+ (black solid) has a band gap at the Fermi energy (red dash at $E–E_f = 0$), representing its semiconducting feature. With a low concentration of Na^+ cations (red solid), the conduction band for the DoS of OMS-5 slightly shifts below the Fermi energy, indicating that electrons are accumulated at the Fermi energy, and OMS-5

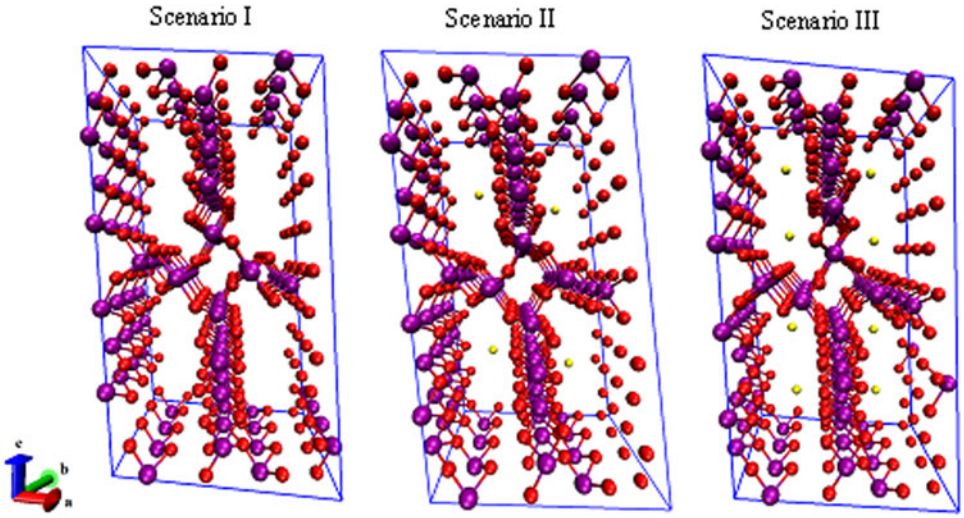

Figure 3. (Color online) Three OMS-5 scenarios our studies focus on, including OMS-5 without cations ($Mn_{96}O_{192}$), with a low concentration of Na^+ cations ($Mn_{96}O_{192}Na_4$), and with a high concentration of Na^+ cations ($Mn_{96}O_{192}Na_8$). Mn in purple, O in red, and Na in gold.

TABLE I. Lattice parameters and tunnel dimensions for OMS-5 without any Na^+ (i.e. Scenario I $Mn_{96}O_{192}$ as a reference), with a low concentration of Na^+ cations (i.e. Scenario II $Mn_{96}O_{192}Na_8$), and a high concentration of Na^+ cations (i.e. Scenario III $Mn_{96}O_{192}Na_8$).

	a (Å)	b (Å)	c (Å)	α	β	γ	Tunnel size $a \times c$ (Å × Å)	Tunnel length b (Å)	Volume (Å^3)
$Mn_{96}O_{192}$	12.343	10.92	23.03	90	97.27	90	4.31 × 9.35	10.92	440.07
$Mn_{96}O_{192}Na_4$	12.358	10.843	23.14	89.98	97.42	89.97	4.31 × 9.39	10.84	438.58
$Mn_{96}O_{192}Na_8$	12.352	10.828	23.14	89.93	97.06	90.01	4.31 × 9.35	10.83	436.35

TABLE II. The calculated formations energies of Na^+ and CO_2 in OMS-5.

	Formation energy of Na^+ (eV/Na^+)
Scenario II: $Mn_{96}O_{192}Na_4$	−2.10
Scenario III: $Mn_{96}O_{192}Na_8$	0.44
	Formation energy of CO_2 (eV/CO_2)
Scenario II: $Mn_{96}O_{192}Na_4 + 4CO_2$	−1.01
Scenario II: $Mn_{96}O_{192}Na_4 + 8CO_2$ "head-to-head"	−1.31
Scenario II: $Mn_{96}O_{192}Na_4 + 8CO_2$ "stacking"	−1.19
Scenario III: $Mn_{96}O_{192}Na_8 + 4CO_2$	−1.01
Scenario III: $Mn_{96}O_{192}Na_8 + 8CO_2$ "head-to-head"	−1.14
Scenario III: $Mn_{96}O_{192}Na_8 + 8CO_2$ "stacking"	−0.78

becomes *n*-type semiconducting. The accumulated electrons are donated from Na^+ cations to OMS-5, resulting in ionic bonds between Na^+ and OMS-5. As the concentration of Na^+ cations increases (blue solid), more electrons donated by Na^+ are accumulated at the Fermi energy.

B. CO_2 adsorption in OMS-5

We then added CO_2 molecules in the OMS-5 with different concentrations of Na^+ cations. We calculated the formation energy of CO_2, DoS, and partial charge density to study the position and orientation of CO_2 adsorbed in the OMS-5, and its interaction with Na^+. Like Na^+ cations, the unit of $Mn_{96}O_{192}$ could accommodate one or two CO_2 molecules in each 2 × 4 tunnel. Table II lists the formation energy of a CO_2 molecule for different scenarios. Generally speaking, its value remains negative, indicating that the adsorption of CO_2 in the OMS-5 is energetically favorable without any energy penalty. As the concentration of CO_2 increases, its formation energy becomes slightly smaller, i.e. more negative and stable. This decrease suggests that CO_2 uptake is energetically favorable before OMS-5 is fully saturated with CO_2. Our future work will examine the "saturation limit" of CO_2. In comparison between one and two Na^+ cations per 2 × 4 tunnel, it is easier to adsorb CO_2 in $Mn_{96}O_{192}Na_4$ than $Mn_{96}O_{192}Na_8$ because of the smaller formation energy and more space available for CO_2. When each 2 × 4 tunnel contains two CO_2 molecules, the formation energy of CO_2 strongly depends on its orientation in the tunnel. Figure 5 illustrates two possible orientations for CO_2 molecules, including head-to-head and stacking orientations. The head-to-head orientation refers to two CO_2 molecules aligning head-to-head along the 2 × 4 tunnel [Figure 5(a)]. The distance between two CO_2 molecules is 3.09 Å. The distances between CO_2 and two neighboring Na^+ cations are 2.76 and 2.63 Å. The stacking is an alternative orientation where two CO_2 molecules stack on top of each other and both align along the 2 × 4 tunnel [Figure 5(b)]. The distance between two CO_2 molecules is 4.06 Å. The distances between the terminal O of CO_2 and two neighboring Na^+ cations are both 2.66 Å. The formation energy for the head-to-head orientation is smaller

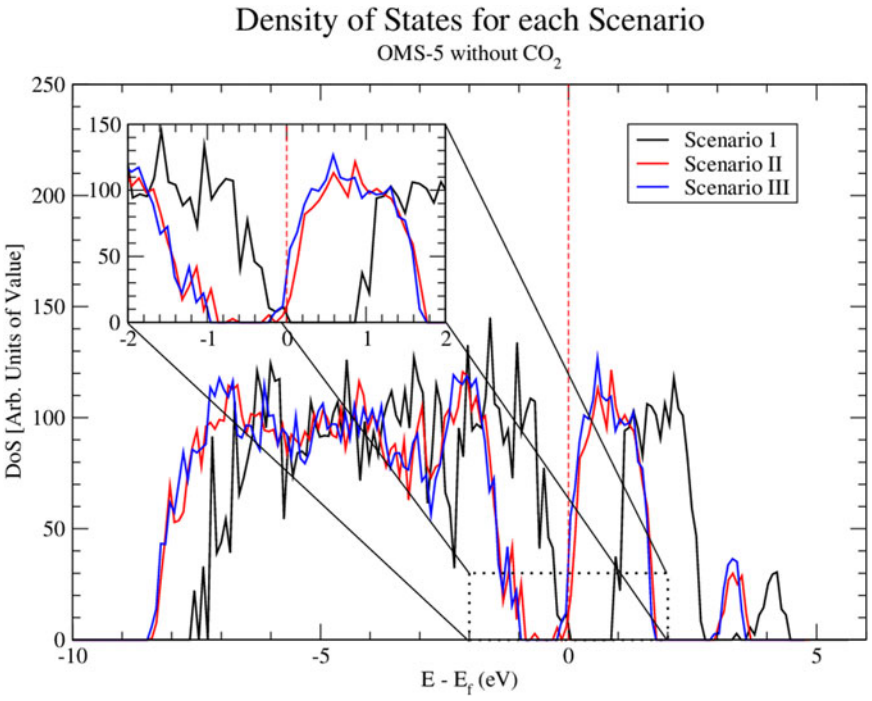

Figure 4. (Color online) Density of states (DoS) for three scenarios. Both $Mn_{96}O_{192}Na_4$ (i.e. Scenario II) and $Mn_{96}O_{192}Na_8$ (i.e. Scenario III) shift the Dos to the lower energy values, compared with $Mn_{96}O_{192}$ (i.e. Scenario I as a reference). The Fermi energy is shown at the dashed red line.

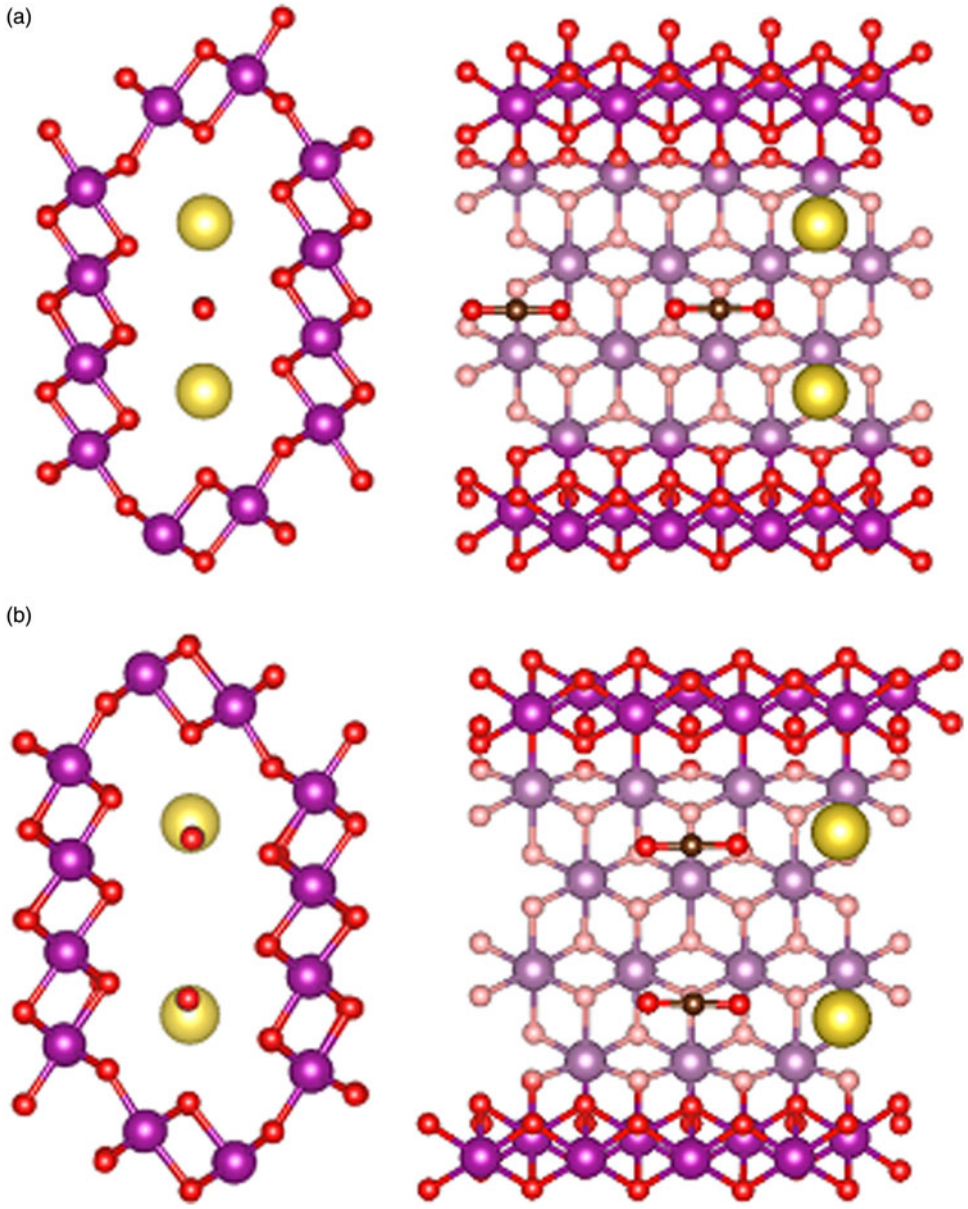

Figure 5. (Color online) Atomic strutures of a single OMS-5 tunnel with Na^+ and CO_2, illustrating (a) "head-to-head" orientation and (b) "stacked" orientation for two CO_2 molecules in the OMS-5 tunnel. Mn in purple, O in red, C in black, and Na in gold.

than that for the stacking orientation in either a low or high concentration of Na^+ cations, suggesting that CO_2 molecules prefer to align head-to-head in the tunnel.

In order to reveal bonding characteristics among CO_2, OMS-5, and Na^+, Figure 4 shows the DoS of OMS-5 for all three scenarios without CO_2. These data confirm that OMS-5 demonstrates semiconducting behavior. Like OMS-2, the DoS of OMS-5 shifts to the lower energy values in the presence of Na^+ cations (Williamson *et al*., 2015). This shift stems from the Na^+ donating electrons to the OMS-5. To examine a CO_2 effect on the electronic structure of OMS-5, electronic DoS and partial charge densities are both shown in Figure 6 for $Mn_{96}O_{192}Na_4 + 8CO_2$ and in Figure 7 for $Mn_{96}O_{192}Na_8 + 8CO_2$ with different concentrations of Na^+ cations but with the same amount of CO_2 molecules. For both configurations, CO_2 molecules align head-to-head along the 2×4 tunnels, as seen in Figure 5a, because the head-to-head orientation is more stable. The DoS figures are projected for $Mn_{96}O_{192}Na_4$ [Figure 6(a)] and $Mn_{96}O_{192}Na_8$ [Figure 7(a)] before and after CO_2 adsorption. Unlike Na^+ cations, the presence of CO_2 molecules does not cause a significant difference in the DoS figures (black and red solid for comparison), suggesting that CO_2 is physically adsorbed in the OMS-5, resulting in a weak bond.

Calculating the partial charge density near the Fermi energy could further explore the bonding characteristics between the CO_2 molecules and OMS-5 framework. Figures 6(b) and 7(b) are the partial charge densities projected along the OMS-5 tunnels in the *b* axis for the valence electrons with the energies of −5 eV to the Fermi energy (i.e. $E–E_f = 0$). Contour lines are drawn to show the regions of equal charge densities. The dark red regions of the OMS-5 framework represent the Mn–O bonds, and are strongly bonded to each other through overlapping contour lines. The partial charge densities of CO_2 molecules are highly localized, so no shared or donated electrons between CO_2 and OMS-5 or

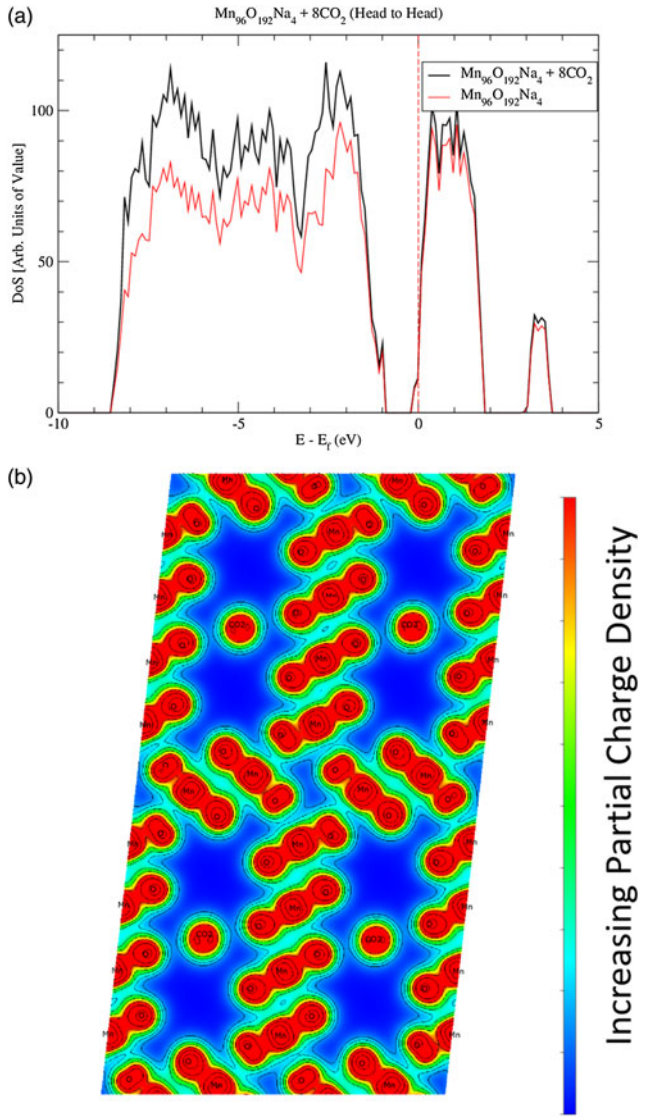

Figure 6. (Color online) Local density of states (a) projecting the contributions of $Mn_{96}O_{192}Na_4 + 8CO_2$ and $Mn_{96}O_{192}Na_4$. The Fermi energy is shown with the dashed line. The partial charge densities (b) for $Mn_{96}O_{192}Na_4 + 8CO_2$ is projected along the OMS-5 tunnels in the *b* axis.

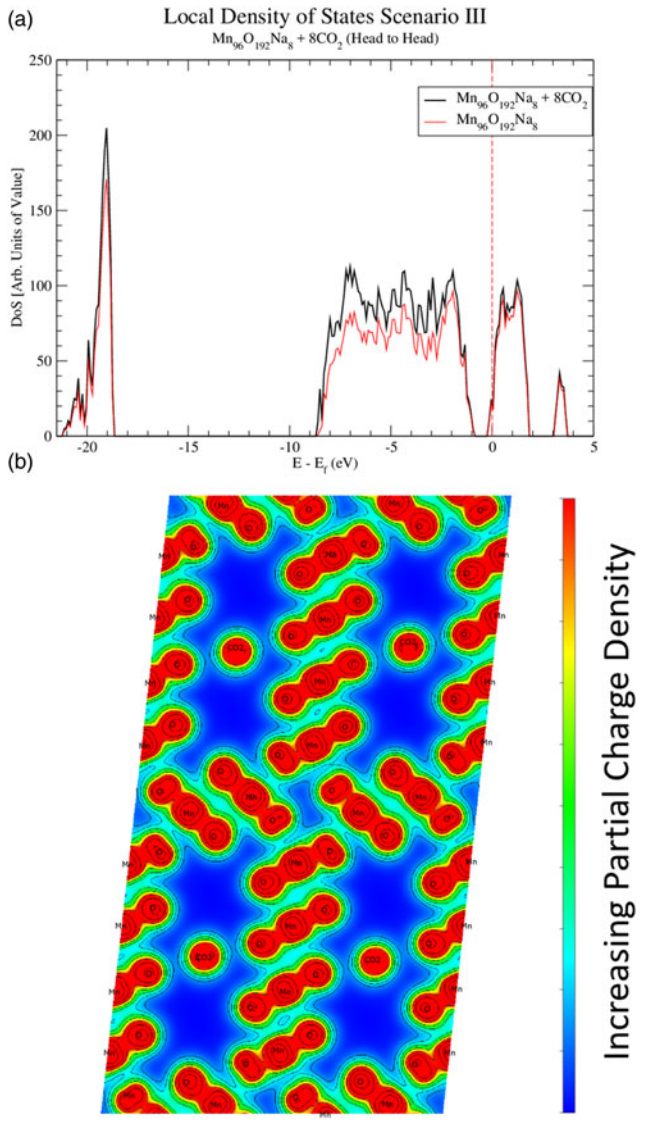

Figure 7. (Color online) Local density of states (a) projecting the contributions of $Mn_{96}O_{192}Na_8 + 8CO_2$ and $Mn_{96}O_{192}Na_8$. The Fermi energy is shown with the dashed line. The partial charge densities (b) for $Mn_{96}O_{192}Na_8 + 8CO_2$ is projected along the OMS-5 tunnel in the *b* axis.

between CO_2 and Na^+ are found. This evidence indicates that CO_2 molecules do not covalently or ionically bond to OMS-5 or Na^+. A weak van der Waals interaction might exist for CO_2 adsorbed in the OMS-5. This type of secondary bonding is much weaker than covalent and ionic bonds. Desorption of CO_2 from the OMS-5 should be easy. Adsorption–desorption hysteresis should also be small. The computational predictions will be validated with our future experiments.

IV. CONCLUSIONS

We utilized DFT-based calculations to understand the structural and electronic properties of OMS-5. The presence of Na^+ cations does not significantly distort the structure of OMS-5. Na^+ ions change the lattice parameters and pore volumes of OMS-5 by <1%. CO_2 adsorption is favorable. According to the analysis of the electronic structure of OMS-5 with Na^+ and CO_2, the Na^+ cations donate electrons to the OMS-5 framework while the CO_2 molecules do not significantly affect the electronic structure of OMS-5. The partial charge densities reveal that the CO_2 molecules are likely captured in the OMS-5 framework through weak van der Waals forces, allowing an easy desorption of CO_2 from the OMS-5. Our studies provide insight into the initial stage and driving force for the adsorption of CO_2 in the OMS-5 series, guiding the OMS materials design for effective carbon capture and storage. For further studies, we will predict CO_2 diffusion mechanisms and estimate CO_2 uptake limits in the OMS-5.

ACKNOWLEDGEMENTS

This research made use of the resources of the High Performance Computing Center at Idaho National Laboratory, which is supported by the Office of Nuclear Energy of the US Department of Energy and the Nuclear Science User Facilities under Contract No. DE-AC07-05ID14517. Further computational resources were provided by the R2 cluster (DOI: 10.18122/B2S41H) administrated by Boise State

University's Research Computing Department. SLS acknowledges the US Department of Energy, Office of Basic Energy Sciences, Division of Chemical, Biological and Geological Sciences under grant DE-FG02-86ER13622.A000.

Botzen, W. J., Gowdy, J. M., and van den Bergh, J. C. (**2008**). "Cumulative CO_2 emissions: shifting international responsibilities for climate debt," Clim.Policy **8**(6), 569–576.

Caskey, S. R., Wong-Foy, A. G., and Matzger, A. J. (**2008**). "Dramatic tuning of carbon dioxide uptake via metal substitution in a coordination polymer with cylindrical pores," J. Am. Chem. Soc. **130**(33), 10870–10871.

Cockayne, E. and Li, L. (**2012**). "First-principles DFT+ U studies of the atomic, electronic, and magnetic structure of α-MnO_2 (cryptomelane)," Chem. Phys. Lett. **544**, 53–58.

D'Alessandro, D. M., Smit, B., and Long, J. R. (**2010**). "Carbon dioxide capture: prospects for new materials," Angew. Chem., Int. Ed. **49**(35), 6058–6082.

DeGuzman, R. N., Shen, Y.-F., Neth, E. J., Suib, S. L., O'Young, C.-L., Levine, S., and Newsam, J. M. (**1994**). "Synthesis and characterization of octahedral molecular sieves (OMS-2) having the hollandite structure," Chem. Mater. **6**(6), 815–821.

Espinal, L., Wong-Ng, W., Kaduk, J. A., Allen, A. J., Snyder, C. R., Chiu, C., and Espinal, A. E. (**2012**). "Time-dependent CO_2 sorption hysteresis in a one-dimensional microporous octahedral molecular sieve," J. Am. Chem. Soc. **134**(18), 7944–7951.

Grimme, S. (**2006**). "Semiempirical GGA-type density functional constructed with a long-range dispersion correction," J. Comput. Chem. **27**(15), 1787–1799.

Holtz-Eakin, D. and Selden, T. M. (**1995**). "Stoking the fires? CO_2 emissions and economic growth," J. Public. Econ. **57**(1), 85–101.

Hou, J., Liu, L., Li, Y., Mao, M., Lv, H., and Zhao, X. (**2013**). "Tuning the K^+ concentration in the tunnel of OMS-2 nanorods leads to a significant enhancement of the catalytic activity for benzene oxidation," Environ. Sci. Technol. **47**(23), 13730–13736.

Jenkinson, D. S., Adams, D., and Wild, A. (**1991**). "Model estimates of CO_2 emissions from soil in response to global warming," Nature **351**(6324), 304.

Lakshmanan, T. and Han, X. (**1997**). "Factors underlying transportation CO_2 emissions in the USA: a decomposition analysis," Transp. Res. D, Transp. Environ. **2**(1), 1–15.

Li, L., Cockayne, E., Williamson, I., Espinal, L., and Wong-Ng, W. (**2013**). "First-principles studies of carbon dioxide adsorption in cryptomelane/hollandite-type manganese dioxide," Chem. Phys. Lett. **580**, 120–125.

Liechtenstein, A., Anisimov, V., and Zaanen, J. (**1995**). "Density-functional theory and strong interactions: orbital ordering in Mott-Hubbard insulators," Phys. Rev. B **52**(8), R5467.

Liu, J., Makwana, V., Cai, J., Suib, S. L., and Aindow, M. (**2003**). "Effects of alkali metal and ammonium cation templates on nanofibrous cryptomelane-type manganese oxide octahedral molecular sieves (OMS-2)," J. Phys. Chem. B **107**(35), 9185–9194.

MacKellar, F. L., Lutz, W., Prinz, C., and Goujon, A. (**1995**). "Population, households, and CO_2 emissions," Popul. Dev. Rev. **21**(4), 849–865.

Perdew, J. P., Burke, K., and Ernzerhof, M. (**1996**). "Generalized gradient approximation made simple," Phys. Rev. Lett. **77**(18), 3865.

Rao, A. B. and Rubin, E. S. (**2002**). "A technical, economic, and environmental assessment of amine-based CO_2 capture technology for power plant greenhouse gas control," Environ. Sci. Technol. **36**(20), 4467–4475.

Raupach, M. R., Marland, G., Ciais, P., Le Quéré, C., Canadell, J. G., Klepper, G., and Field, C. B. (**2007**). "Global and regional drivers of accelerating CO_2 emissions," Proc. Natl. Acad. Sci. USA **104**(24), 10288–10293.

Rochelle, G. T. (**2009**). "Amine scrubbing for CO_2 capture," Science **325**(5948), 1652–1654.

Shen, Y., Zerger, R., DeGuzman, R., Suib, S., McCurdy, L., Potter, D., and O'young, C. (**1993**). "Manganese oxide octahedral molecular sieves: preparation, characterization, and applications," Science **260**(5107), 511–515.

Shen, X. F., Ding, Y. S., Liu, J., Cai, J., Laubernds, K., Zerger, R. P., and Suib, S. L. (**2005**). "Control of nanometer-scale tunnel sizes of porous manganese oxide octahedral molecular sieve nanomaterials," Adv. Mater. **17**(7), 805–809.

Suib, S. L. (**1998**). "Microporous manganese oxides," Curr. Opin. Solid State Mater. Sci. **3**(1), 63–70.

Suib, S. L. and Iton, L. E. (**1994**). "Magnetic studies of manganese oxide octahedral molecular sieves: a new class of spin glasses," Chem. Mater. **6**(4), 429–433.

Williamson, I., Nelson, E. B., and Li, L. (**2015**). "Carbon dioxide sorption in a nanoporous octahedral molecular sieve," J. Phys. D: Appl. Phys. **48**(33), 335304.

Zhang, X., Sun, X., Zhang, H., Li, C., and Ma, Y. (**2014**). "Comparative performance of birnessite-type MnO_2 nanoplates and octahedral molecular sieve (OMS-5) nanobelts of manganese dioxide as electrode materials for supercapacitor application," Electrochim. Acta **132**, 315–322.